

Accepted Manuscript

A novel microstructural design to improve the oxidation resistance of ZrB₂-SiC ultra-high temperature ceramics (UHTCs)

Haiwen Zhang, D.D. Jayaseelan, I. Bogomol, M.J. Reece, Chunfeng Hu, S. Grasso, W.E. Lee

PII: S0925-8388(19)30217-8

DOI: <https://doi.org/10.1016/j.jallcom.2019.01.208>

Reference: JALCOM 49246

To appear in: *Journal of Alloys and Compounds*

Received Date: 19 November 2018

Revised Date: 12 January 2019

Accepted Date: 16 January 2019

Please cite this article as: H. Zhang, D.D. Jayaseelan, I. Bogomol, M.J. Reece, C. Hu, S. Grasso, W.E. Lee, A novel microstructural design to improve the oxidation resistance of ZrB₂-SiC ultra-high temperature ceramics (UHTCs), *Journal of Alloys and Compounds* (2019), doi: <https://doi.org/10.1016/j.jallcom.2019.01.208>.

This is a PDF file of an unedited manuscript that has been accepted for publication. As a service to our customers we are providing this early version of the manuscript. The manuscript will undergo copyediting, typesetting, and review of the resulting proof before it is published in its final form. Please note that during the production process errors may be discovered which could affect the content, and all legal disclaimers that apply to the journal pertain.



A novel microstructural design to improve the oxidation resistance of**ZrB₂-SiC ultra-high temperature ceramics (UHTCs)**

Haiwen Zhang^a, D.D. Jayaseelan,^b I. Bogomol^c, M.J. Reece^d
Chunfeng Hu^{a,*}, S.Grasso^{a,*} and W.E. Lee^e

^a*Key Laboratory of Advanced Technologies of Materials, Ministry of Education,
School of Materials Science and Engineering, Southwest Jiaotong University,
Chengdu 610031, China*

^b*Department of Aircraft and Aerospace Engineering, Kingston University of London,
SW15 3DW, United Kingdom*

^c*National Technical University of Ukraine "KPI", Peremogy av. 37, Kyiv 03056
Ukraine*

^d*Queen Mary University of London, UK*

^e*Centre for Advanced Structural Ceramics, Department of Materials,
Imperial College London, UK, SW7 2AZ*

*Corresponding authors: Prof. Salvatore Grasso and Chunfeng Hu

School of Materials Science and Engineering

Southwest Jiaotong University

Chengdu 610031, China

E-mail addresses: s.grasso@swjtu.edu.cn (S. Grasso) and chfhu@live.cn (C. Hu)

Abstract

Directionally Solidified 72.8 mol% ZrB₂ - 27.2 mol% SiC (equivalent to 20 vol%) composite was fabricated using a crucibleless-melting technique. Microstructural and XRD analyses confirmed the texturing of grains and lamellar structure. The Lotgering (001) orientation factor was as high as 0.97. The thickness of the lamellae was about 5 μm. Bright-field TEM images confirmed that the eutectic composite has continuous ZrB₂ and SiC phases. Electron diffraction patterns from both the ZrB₂ and SiC phases were indexed as hexagonal and 3C-cubic structures, respectively. Line defects such as dislocations, stacking faults and twins were observed in the SiC. Oxidation studies performed at 1873K for 1h demonstrated that the samples obtained by melting showed an improved oxidation resistance compared to ZrB₂-SiC composites obtained via sintering due to the formation of a passivating continuous SiO₂ layer. The oxidation mechanisms are discussed, the orientation and SiC lamellae as acted as an

effective barrier to the inward oxygen flux and played a key role in retarding oxidation.

Key words: Eutectic structure; ZrB_2 -SiC; microstructure; oxidation

Introduction

Ultra high temperature ceramics (UHTCs) are candidate materials for a variety of aerospace applications owing to their unique combination of properties, including high melting temperature ($>3273K$), high strength, and high elastic modulus[1–5]. However, their oxidation resistance (especially for additive free materials) is a major issue in the development of transition metal boride based UHTCs for high temperature applications as the oxidation product B_2O_3 evaporates resulting in a porous and non-protective columnar ZrO_2 or HfO_2 grain structure.[6–9]

Most developments to increase the oxidation resistance of UHTCs are based on the addition of 20-30 vol% SiC to produce a protective silica (silicate) layer on the surface during oxidation. To further improve the oxidation resistance of ZrB_2 /SiC composites, transition metal borides such as TiB_2 , TaB_2 and VB_2 have been added.[10–12] Other approaches adopted to enhance the oxidation resistance include adding silicides, which increase the viscosity of the liquid silica layer[13–17] by making the different liquid phases immiscible.[10–12] Another approach is to fabricate dense ZrO_2 layers via liquid phase sintering, thus reducing oxygen penetration and its diffusivity.[18,19]

Using a different approach, the *in-situ* development of solid refractory oxide protective layers by adding rare earth (RE) oxides to ZrB_2 /SiC composites was also proposed in Refs.[20,21] Addition of RE oxides formed RE zirconates as an outer protective layer that has higher melting point and lower oxygen diffusivity when compared with silicates or oxides. Chen *et al.* developed the eutectic composition of LaB_6 - ZrB_2 and investigated its oxidation behaviour.[22] It was expected that the absence of low energy grain boundaries in the eutectic microstructure would contribute to improved oxidation resistance. However, the oxidation studies at high

temperatures showed that the Directionally Solidified (DS) $\text{LaB}_6\text{-ZrB}_2$ was not a sustainable candidate for UHT applications in air because of its poor oxidation resistance in spite of its excellent creep resistance and other mechanical properties.[22] Directionally Solidified $\text{LaB}_6\text{-ZrB}_2$ exhibited parabolic oxidation kinetics below 1373K with 80 minutes holding time and behaved para-linearly above this temperature due to the rapid evaporation of B_2O_3 and the separation and run-off of lanthanum borate liquid in the scale, which offered less of a barrier to oxygen diffusion. Furthermore, preferential oxidation of LaB_6 occurred in the composite and appeared more aggressive at low oxygen partial pressures.

Although previous oxidation results on DS UHTCs were not encouraging,[22] it is expected that DS materials might exhibit better oxidation resistance at high temperatures. Melt grown eutectics have microstructures with a three-dimensional continuous network of elongated mono-crystal phases without grain boundaries. At present, various microstructure design techniques have been employed to fabricate textured ZrB_2 -based ceramics. These methods include: hot forging;[23] template grain growth;[24] strong magnetic field alignment;[25] and melt solidification.[26] Among all these methods, the oxidation resistance of materials produced via melt solidification has not yet been reported. For this reason, this work was focused on textured materials obtained via melt solidification.

Experimental Details

The DS composite was produced by a floating zone method based on crucibleless zone melting of the compacted powders as described by Loboda[27]. Cylindrical billets of powder mixtures of ZrB_2 SiC, and boron 10 mm in diameter and 140 mm long (porosity 35- 40%) were compacted using uniaxial pressing. The ingots were subjected to zone melting with induction heating in a Kristall-206 unit in an atmosphere of ultrapure helium (99.999 mass%) at a pressure of 1 atm. The billet was melt using an induction heating at a rate of about 1000 K/min under constant power, the speed of movement (relative to the inductor) was 2 mm per minute. Directionally solidified $\text{ZrB}_2\text{-SiC}$ with a molar composition of 80:20 vol% and a

relative density close to 99% was obtained. ZrB₂ Grade B with average particle size of 2.4 μm supplied by Starck (Germany) containing impurities of C 0.13; O 0.8; N 0.21; Hf 1.77, wt % was used as starting material. The SiC starting powder used for this investigation was UF-10 α-SiC with average particle size of 0.7 μm produced by H.C. Starck (Germany). The purity of the starting powder was 98.5 wt%. The main impurities were O (<1.1 wt%), Al (<0.03 wt%), Ca (<0.01 wt%) and Fe (<0.05 wt%). The bulk density of sintered samples was measured using the Archimedes' method with distilled water as the immersion fluid and the theoretical density was calculated from the rule of mixtures.

Spark plasma Sintering experiments was done using an SPS furnace (FCT HPD 25; FCT Systeme GmbH) under vacuum (~5 Pa), heating rate was 100 K/min dwell time at 2373 K of 10 minutes and pressure of 40 MPa.

The oxidation studies of the DS ZrB₂-SiC sample were carried out using a conventional open-hearth bottom loading furnace. Rectangular bars of dimension 4 x 5 x 5 mm³ machined from a DS ZrB₂-SiC ingot were placed on an alumina boat so that there was minimal contact to maximise airflow over the samples. In the TG-DTA experiments, a rectangular bar of same size (4 x 5 x 5 mm³) was kept standing vertically along the airflow. Phase analysis was conducted for zone melted ZrB₂-SiC samples before and after oxidation with X-ray diffraction (PANalytical MRD; Almelo, The Netherlands). X-ray diffraction signals were collected using Cu Kα radiation and measured with a 0.03° step. The samples tested for oxidation had relative density of 99% and were prepared from the same starting powders.

Samples for scanning electron microscopy (SEM) were mounted in epoxy resin and polished in successive steps using diamond composite discs and slurries. In addition, a final polishing step was conducted using a vibratory polishing machine (VibroMet 2, Buehler; Lake Bluff, Ill., USA) for 24 h. Microstructural analysis was performed using a scanning electron microscope (Auriga, Carl Zeiss; Oberkochen, Germany). Backscattered electron (BSE) and secondary electron (SE) images were taken at an acceleration voltage of 15 kV and elemental analysis conducted using an Energy Dispersive Spectroscopy (EDS) unit (X-Max 20, Oxford instruments;

Abingdon, UK). Samples of 3 mm diameter were cut from the zone melted sample and polished to 30 μm thickness using a disc grinder, dimpled using a dimple grinder (Gatan 656 Dimple Grinder, Abingdon, UK) with 1 μm paste to a thickness of <10 μm and ion-polished using a Precision Ion Polishing System (PIPS, Gatan 691, Abingdon, UK) to an electron-transparent finish. Transmission electron microscopy (TEM) analysis was conducted at an operating voltage of 200 kV using a JEOL FX2100 (Tokyo, Japan) fitted with EDS (X-Max 80, Oxford instruments; Abingdon, UK). Selected area electron diffraction (SAED) patterns were indexed using single crystal diffraction patterns from Williams and Carter[9] and TEM diffraction analysis software (SingleCrystal, CrystalMaker Software Ltd.; Begbroke, UK).

Results and Discussion

Figure 1 shows the phase diagram of $\text{ZrB}_2\text{-SiC}$. Tu *et al.*[28] fabricated a series of compositions of DS $\text{ZrB}_2\text{-SiC}$ samples and demonstrated that there is a eutectic composition at 58.5 mol% ZrB_2 -41.5 mol% SiC. A eutectic composition with close to 50mol % composition tends to produce a more homogeneous eutectic structure. In the present study, the reference composition of 72.8 mol% ZrB_2 - 27.2 mol% SiC (20 vol% SiC), which has been widely used in most of the previous studies on UHTCs, was investigated.

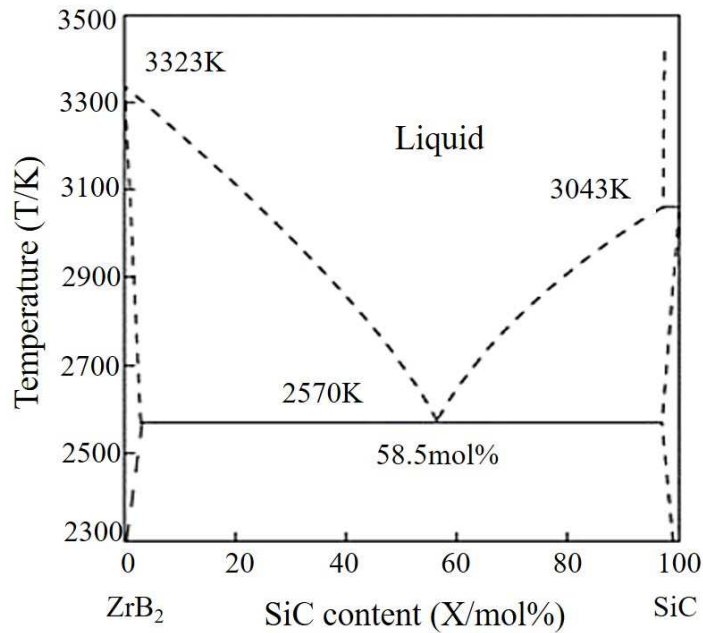


Figure 1 Phase diagram of $\text{ZrB}_2\text{-SiC}$ [23]Eutectic composition: 41.5 ZrB_2 - 58.5 SiC (mol%); Eutectic melting point: 2570 K.

An ingot obtained using crucibleless zone melting technique is shown in Figure 2, the cross section was 6 mm in diameter and the length was 60 mm. The zone-melted $\text{ZrB}_2\text{-SiC}$ sample was nearly 99% of theoretical density. Figure 3 shows BSE images of an ingot at the ipoeutectic composition of 72.8 mol% ZrB_2 - 27.2 mol% SiC melt grown parallel (Figure 3(a)) and perpendicular (Figure 3(b)) to the growth direction, which is the c -axis of ZrB_2 . The $\text{ZrB}_2\text{-SiC}$ eutectic consisted of uniformly distributed and aligned ZrB_2 and SiC phases. In Figure 3(b) eutectic regions (red arrows) and ZrB_2 rich regions (blue arrows) are evidenced. The texturing of grains is evidently seen in the SEM image taken parallel to the growth direction (Figure 3(a)). The continuity of the two different contrasting phases is well evident. The dark phase is SiC and the bright phase is ZrB_2 . Phase analysis of the zone-melted sample using XRD (Figure 4) confirmed the significant texturing observed in the SEM images. The top of the sample shows a very high intensity of the diffraction ($00l$) peaks for the ZrB_2 and SiC , while the side of the sample shows preferential (100) ZrB_2 diffraction peaks. The high level of texturing is produced by the thermal gradients generated in the process. The ($00l$) Lotgering orientation factor was as high as 0.97.



Figure 2 Crucibleless zone-melted $\text{ZrB}_2\text{-SiC}$ sample (27.2 mol% SiC)

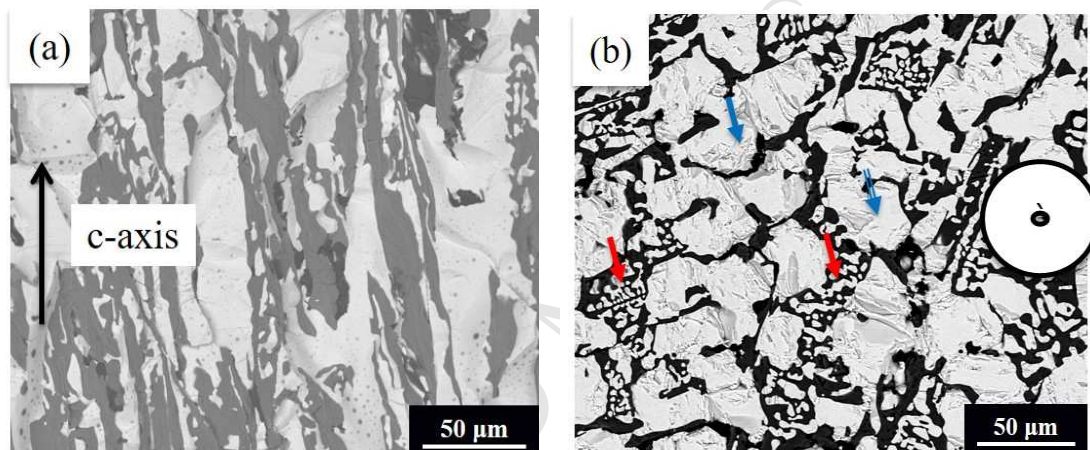


Figure 3 Back-scattered electron image of a DS $\text{ZrB}_2\text{-SiC}$ sample (a) side view and (b) top view (c-axis) (as described in inset in figure 5). The red arrows point at the eutectic region while blue arrows point at the ZrB_2 rich region which is the primary phase formed during the cooling from the melt.

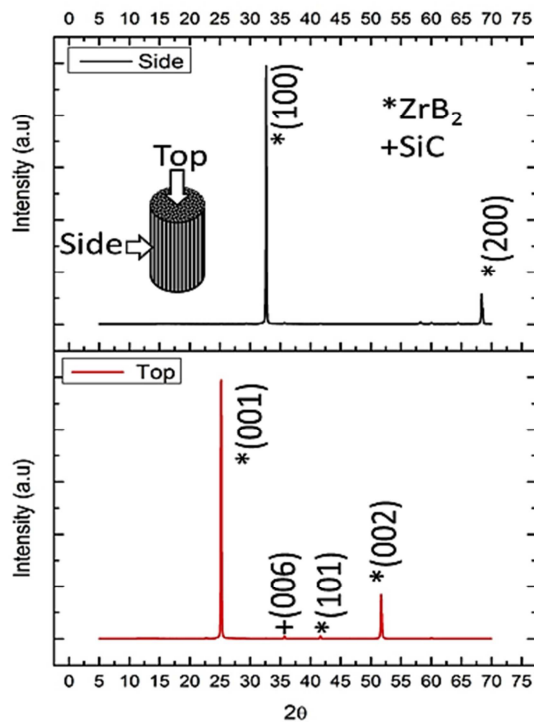


Figure 4 XRD patterns from the side and top surfaces of the DS sample are also shown. The inset clarifies the sample orientation.

Figure 5 shows a bright field TEM image of the ZrB_2 -SiC eutectic made by the melting technique. The bright phase is SiC and the dark phase is ZrB_2 . The lamella thickness is about 5 μm . SAEDs were taken from regions labeled (a) (b) (c) and (d) in Fig. 5. SAEDs of the SiC phase along the [111] zone axis can be indexed as cubic and corresponds to the 3C-SiC polytype (β -SiC) in the eutectic composition. Although, the SAEDs were taken from different regions, all of them have the same orientation, which confirms the single crystalline nature of the lamellae. Similarly, SAEDs taken from regions (c) (d) and E along the [0001] zone axis confirm the hexagonal symmetry of the ZrB_2 grains. HRTEM of a ZrB_2 -SiC interface is shown in Figure (e), revealing an impurity-free grain boundary. The level of crystallographic misorientation is minimal and this is a typical feature of DS materials, resulting in low energy grain boundaries.

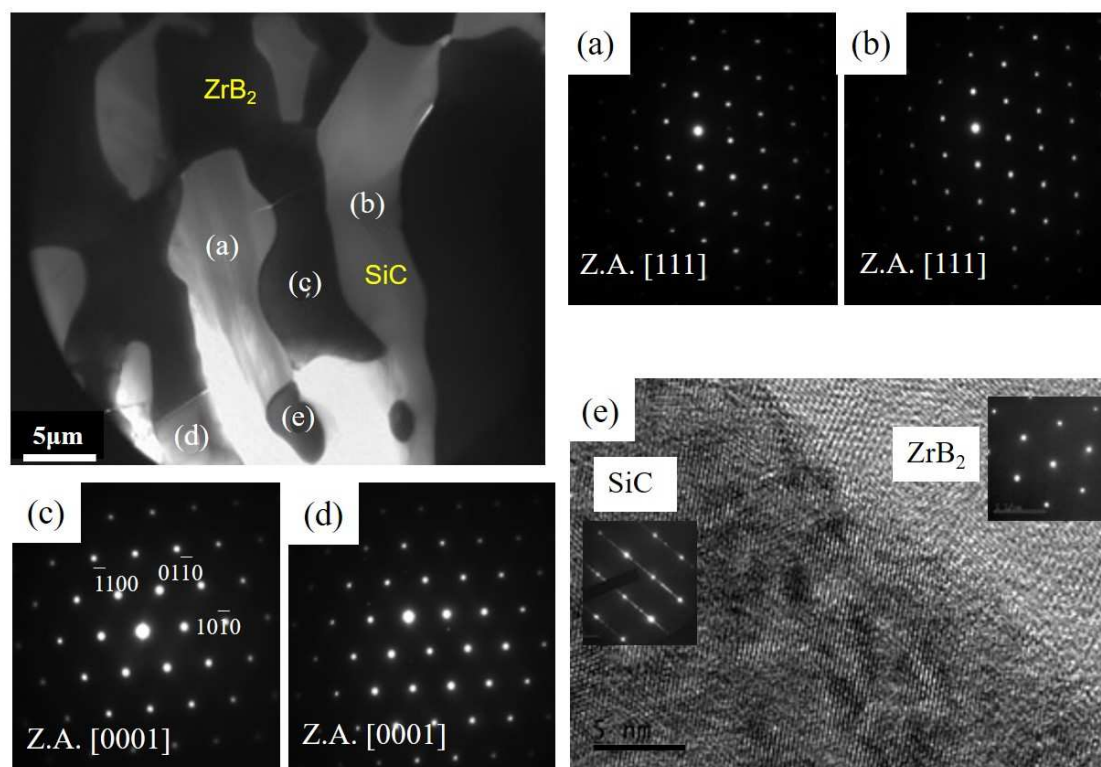


Figure 5 Bright-field(BF)TEM image of DS ZrB_2 -SiC respective regions in brackets corresponds to: (a) and (b) are SiC and (c),(d) and (e) are ZrB_2 ; (a) , (b) – SAED taken from the labeled regions of (a) and (b), respectively in the zone axis [111] in the BF; TEM image (c),(d) – SAED taken from the labeled regions of (c) and (d), respectively in the zone axis [0001] in the BF; TEM image (e) - High resolution TEM image of a ZrB_2 -SiC interface showing clean boundary and corresponding SAEDs taken from respective region.

Figure 6a shows a typical bright-field TEM image of a ZrB_2 -SiC DS sample observed in another region of the sample. SiC is sandwiched between dark ZrB_2 regions. A high magnification image of the square drawn in Fig.6(a) is shown in Fig. 6(b). The bright-field TEM image reveals bend contours, which can be an artifact of the sample preparation or produced by internal stresses. EDS analysis of the region in the square confirms it as SiC. SAEDs were taken from different regions within the square. Figure 6(c) is an SAED taken along the [111] zone axis, confirming cubic β -SiC. The double diffraction spots in the SAED pattern shown in Fig.6(d) might be attributed to twins or they could be produced by the epitaxial mixing of different polytypes, which is common in SiC. The streaking in the SAED confirms the presence of stacking

faults. Figure 6(e) shows the SAED taken from a SiC grain in a different region. The SAED shows a superlattice structure, which could be indexed as 6H-SiC. This observation shows that during rapid solidification SiC may crystallise into different polytypes. DS phases are grown directly from the melt at very high temperature above 3000°C, and the eutectic reaction leads to the nucleation of two phases with strong interfacial bonding and different thermal expansion coefficients ($\text{SiC} - 4 \times 10^{-6}/^\circ\text{C}$ and $\text{ZrB}_2 - 6.7 \times 10^{-6}/^\circ\text{C}$). The thermal expansion mismatch between ZrB_2 and SiC induced thermal strains as the material cools, which cannot be relaxed because plastic deformation in the ceramic is limited, giving rise to large thermal residual stresses.

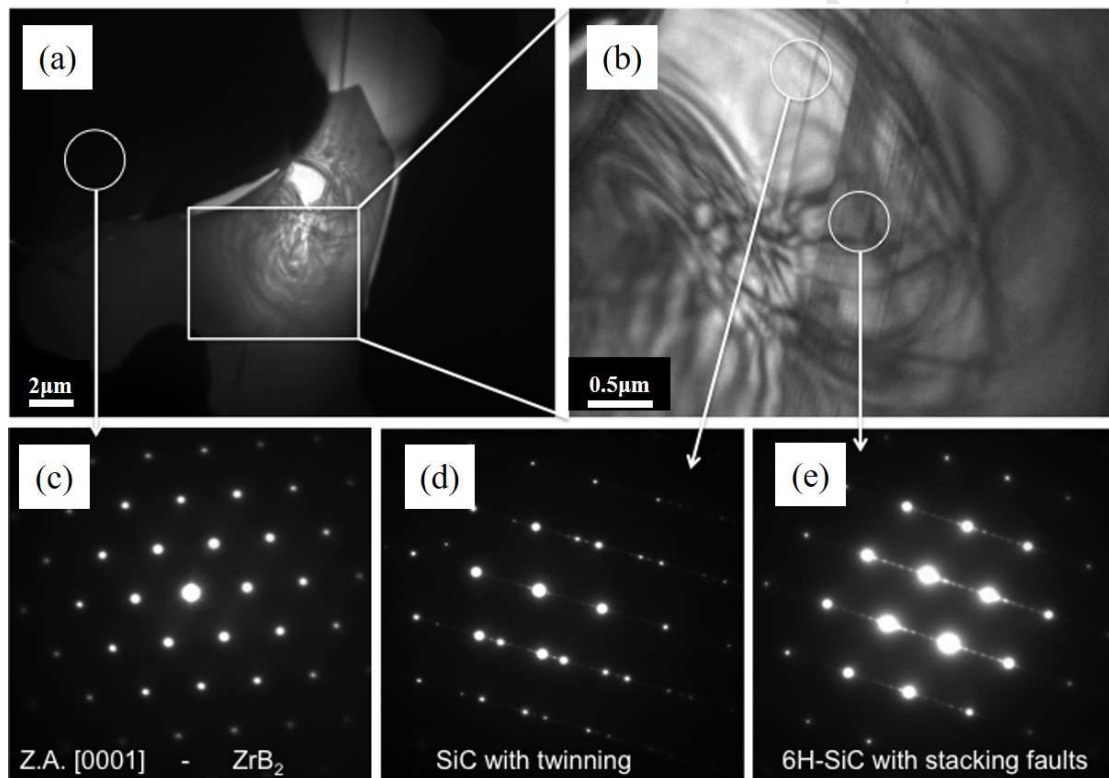


Figure 6 Bright field images of DS ZrB_2 -SiC and corresponding SAEDs.

Oxidation studies

The oxidation studies of DS ZrB_2 -SiC were carried out using a conventional furnace at temperatures up to 1600°C with 1h holding. With the aim of identifying the role of processing with respect to the oxidation resistance, samples made with different processing techniques (DS sample, and sample obtained by SPS of milled as received powders, sample obtained by SPS of powder derived from crushed DS ingots) were

studied.

The surface microstructures of the DS $\text{ZrB}_2\text{-SiC}$ oxidised at 1873K for 1h are shown in Fig.7. The surfaces are smooth and there are some differences in the surface morphology depending on the sample orientation. The number bright zirconia particles in Figure (b) is crealy larger than in Figure (a). The bright rounded grains are zirconia (EDX spot A) while the dark smooth surface is silica (EDX spot B)). Individual zirconia grains are surrounded by a silica film. In the DS $\text{ZrB}_2\text{-SiC}$ ingot, both ZrB_2 and SiC phases are interlayered and homogeneously distributed. During oxidation, ZrB_2 oxidizes to ZrO_2 and B_2O_3 above 1073K. With further increase in temperature, SiC oxidises to SiO_2 and CO_2 . B_2O_3 can either react with silica to form borosilicate glass and form a protective film around individual ZrO_2 grains, if B_2O_3 is not available locally silica by itself can form a protective silica glass. The side of the sample contains a prevalence of silica, while the top section has a prevalence of zirconia. This can be explained by looking at the microstructure of a DS sample (Figure 3 (a) and (b)) where on the side there is a continuous SiC layer which is converted to silica (Figure 8 (a)), while on the top surface ZrB_2 is converted in zirconia (Figure 8 (b)).

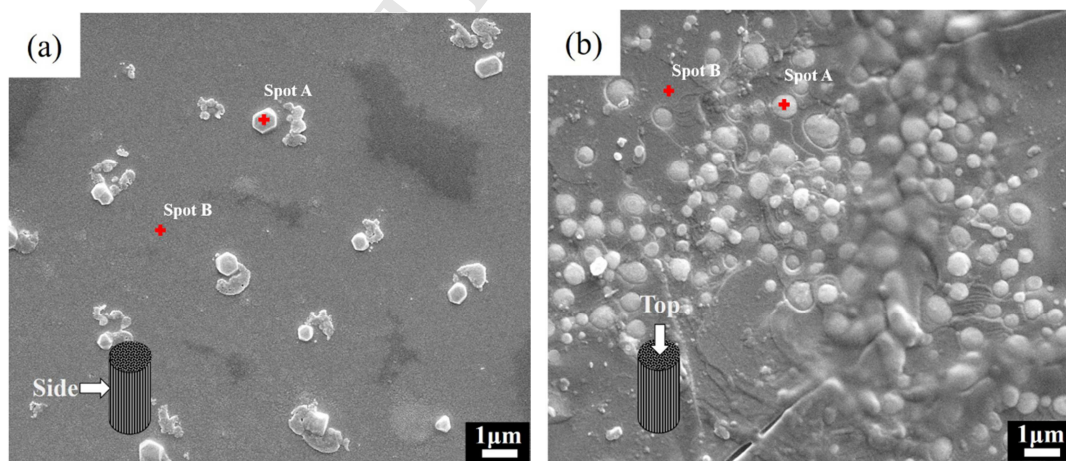


Figure 7 SEM of oxidised surface of DS $\text{ZrB}_2\text{-SiC}$ for 1h at 1873K: (a) side and (b) top views. The white arrows shows the sample surface subjected to oxidation.

Figure 8 shows polished cross-sections showing the microstructure of $\text{ZrB}_2\text{-SiC}$ after oxidation for 1h at 1873K prepared using different techniques. The measured oxide scales is given in table 1. Fig 8(a) shows a thin ($< 65 \mu\text{m}$) oxygen-rich layer is formed on the side of DS sample. The lamellae orientation has a strong effect on the oxidation resistance because the continuous layer of SiC facing the inward oxygen diffusion resulted in formation of a silica layer which was an effective barrier. The formation of a SiC continuous lamella of the DS sample side was promoted by the preferential solidification of SiC because of its lower melting/decomposition temperature compared ZrB_2 .

On the top side the zirconia layer did not offer effective protection against oxidation and the scale thickness was about $205 \mu\text{m}$, which is comparable to that reported for pure ZrB_2 . [29] A sample prepared by crushing DS samples prepared as detailed in Ref.[30] have a random orientation with respect to the inward oxygen flux. The scale formed on this sample was $160 \mu\text{m}$ thick, as expected this thickness is intermediate between that for the DS top and its side. Comparing all of the DS samples seen in Figures 8 reveals that the SiC front facing the inward oxygen flux has a dominant role in controlling the thickness of the oxide layer. According to Zhu et al.[31] the oxidation resistance in $\text{ZrB}_2\text{-SiC}$ is improved by having finely dispersed (distance between SiC particles of about $10 \mu\text{m}$) SiC particles in the matrix because of the improved tendency of fine particles ($<3 \mu\text{m}$) to form a continuous silica protective layer. As a result the SPS samples prepared at 2373 K results had a scale thickness of $80 \mu\text{m}$. Cross sections of solid state sintered samples had a morphology of the scale similar to that described in a recent review.[32] The sample side had quite a distinctive oxidation behavior which was not previously reported as the oxygen inward flux was retarded by the SiC/ ZrB_2 lamellar structure. The composition of borosilicate glass formed during the oxidation product is difficult to determine because of the difficulties in measuring B content. On the side surface the silica layer the layer formed from SiC continuous lamella is likely to contain a reduced boron

content.

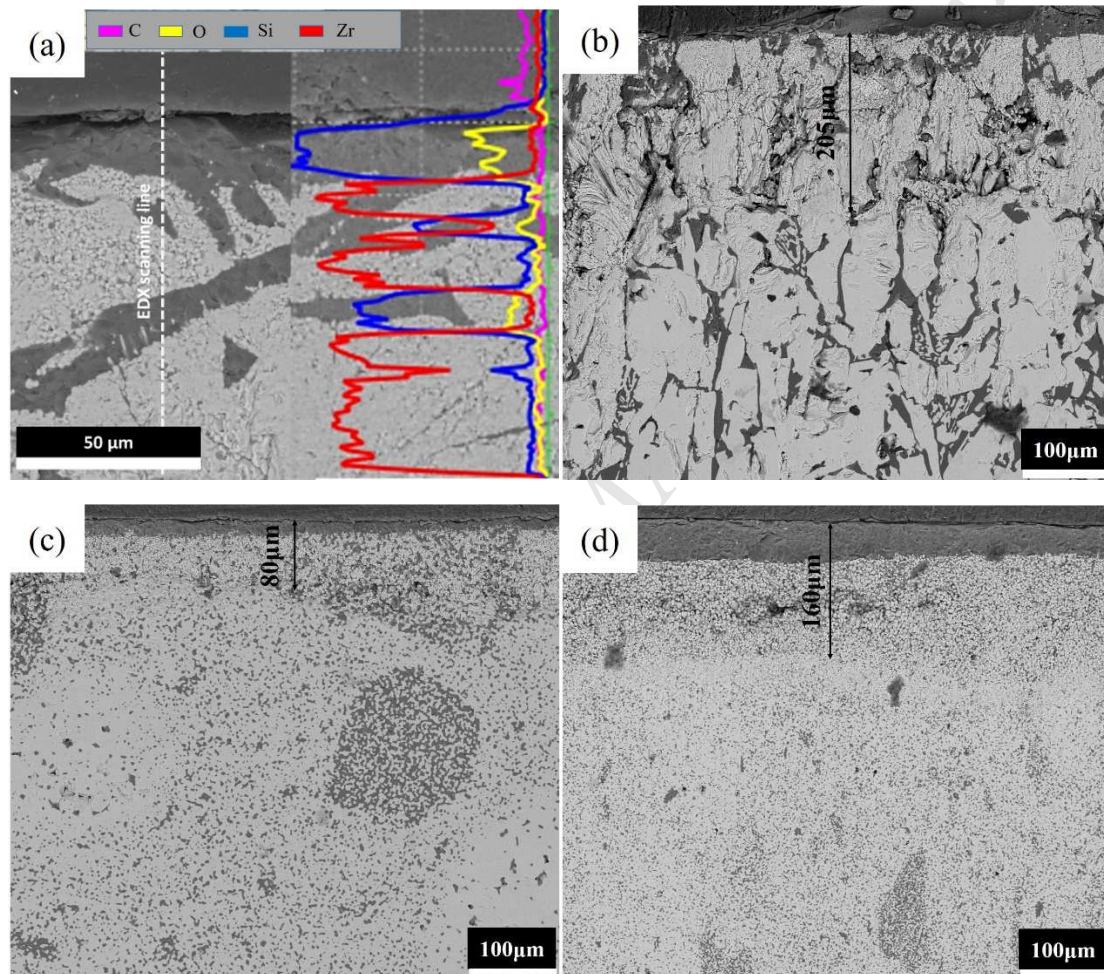


Figure 8 Comparison of oxidation oxide scale (top side of the figure) of 20vol%SiC-ZrB₂ after oxidation at 1873K for 1 h. Samples were processed using various techniques: (a) Side of the DS sample with overlapped EDX mapping, (b) Top of DS sample, (c) sample obtained by SPS of milled as received powders (d) sample obtained by SPS of powder derived from crushed DS ingots. High magnification images are available in the supplementary section.

Table 1 Oxidation layer thickness of UHTC samples after 1h oxidation in air at 1873K.

Sample	Oxidation Layer Thickness (μm)
--------	--------------------------------

ZrB ₂ /SiC(the top of DS sample)	205±3.8
ZrB ₂ /SiC(the side of DS sample)	65±4.3
ZrB ₂ /SiC(SPS sample)	80±5.1
ZrB ₂ /SiC(DS+SPS sample)	160±3.2

Conclusions

A novel design of a eutectic engineered microstructure improved the oxidation resistance of ultra-high temperature ceramic (UHTC) composites. Oxidation studies of solidified melt processed ZrB₂-SiC with eutectic microstructures show that they could guide the design of UHTCs with improved oxidation resistance. The silica protective layer formed in directional solidified specimen was continuous and it was formed by the oxidation of SiC layers. Melt processing could add a further degree of freedom in designing the properties of UHTCs, in particular, low energy grain boundaries might further improve oxidation resistance.

References

- [1] W.G. Fahrenholtz, G.E. Hilmas, I.G. Talmy, J.A. Zaykoski, Refractory diborides of Zirconium and Hafnium, *J. Am. Ceram. Soc.* 90 (2010) 1347–1364.
- [2] J.W. Zimmermann, G.E. Hilmas, W.G. Fahrenholtz, F. Monteverde, A. Bellosi, Fabrication and properties of reactively hot pressed ZrB₂-SiC ceramics, *J. Eur. Ceram. Soc.* 27 (2007) 2729–2736.
- [3] S.Q. Guo, Densification of ZrB₂-based composites and their mechanical and physical properties: A review, *J. Eur. Ceram. Soc.* 29 (2009) 995–1011.
- [4] R. Savino, M.D.S. Fumo, D. Paterna, M. Serpico, Aerothermodynamic study of UHTC-based thermal protection systems, *Aerosp. Sci. Technol.* 9 (2005) 151–160.
- [5] M.M. Opeka, I.G. Talmy, E.J. Wuchina, J.A. Zaykoski, S.J. Causey, Mechanical, thermal, and oxidation properties of refractory hafnium and

- zirconium compounds, *J. Eur. Ceram. Soc.* 19 (1999) 2405–2414.
- [6] T.A. Parthasarathy, R.A. Rapp, M. Opeka, R.J. Kerans, A model for the oxidation of ZrB_2 , HfB_2 and TiB_2 (Postprint), *Acta Mater.* 55 (2007) 5999–6010.
- [7] T.A. Parthasarathy, R.A. Rapp, M. Opeka, R.J. Kerans, Effect of phase change and oxygen permeability in oxide scales on oxidation kinetics of ZrB_2 and HfB_2 , *J. Am. Ceram. Soc.* 92 (2010) 1079–1086.
- [8] F. Monteverde, I. National, A. Bellosi, I. National, Oxidation of ZrB_2 based ceramics in air oxidation of ZrB_2 -based ceramics in dry air, *J Electrochem Soc.* 150 (2003) B552-B9.
- [9] Tripp, W.C, Graham, H.C, Thermogravimetric study of oxidation of ZrB_2 in temperature range of 800°C to 1500°C, *J Electrochem Soc.* 118 (1971) 1195-1199.
- [10] E. Eakins, D.D. Jayaseelan, W.E. Lee, Toward oxidation-resistant ZrB_2 -SiC ultra high temperature ceramics, *Metall. Mater. Trans. A.* 42 (2011) 878–887.
- [11] D.W. Mckee, C.L. Spiro, E.J. Lamby, The effects of boron additives on the oxidation behavior of carbons, *Carbon N. Y.* 22 (1984) 507–511.
- [12] I.G. Talmy, J.A. Zaykoski, M.M. Opeka, High temperature chemistry and oxidation of ZrB_2 ceramics containing SiC, Si_3N_4 , Ta_5Si_3 , and $TaSi_2$, *J. Am. Ceram. Soc.* 91 (2010) 2250–2257.
- [13] V. BG., A structural model of immiscibility of silicate glass-forming melts, *Glas. Phys. Chem.* 19 (1993) 218–225.
- [14] V. BG., Two-phase glasses: structure, properties, and applications, *Nauk. Leningr.* (1991).
- [15] T.H. Kuchino J, Kurokawa K, Shibayama T, Effect of microstructure on oxidation resistance of $MoSi_2$ fabricated by spark plasma sintering, *Vacuum.* 73 (2004) 623–628.
- [16] S.N. Karlsdottir, J.W. Halloran, Formation of oxide scales on zirconium diboride–silicon carbide composites during oxidation: relation of subscale recession to liquid oxide flow, *J. Am. Ceram. Soc.* 91 (2010) 3652–3658.

- [17] S.N. Karlsdottir, J.W. Halloran, C.E. Henderson, Convection patterns in liquid oxide films on ZrB_2 -SiC composites oxidized at a high temperature., *J. Am. Ceram. Soc.* 90 (2007) 2863–2867.
- [18] E. Opila, S. Levine, J. Lorincz, Oxidation of ZrB_2 - and HfB_2 -based ultra-high temperature ceramics: Effect of Ta additions, *J. Mater. Sci.* 39 (2004) 5969–5977.
- [19] S.C. Zhang, G.E. Hilmas, W.G. Fahrenholtz, Improved oxidation resistance of zirconium diboride by tungsten carbide additions, *J. Am. Ceram. Soc.* 91 (2010) 3530–3535.
- [20] D.D. Jayaseelan, E. Zapata-Solvas, P. Brown, W.E. Lee, J. Halloran, In situ formation of oxidation resistant refractory coatings on SiC reinforced ZrB_2 ultra high temperature ceramics, *J. Am. Ceram. Soc.* 95 (2012) 1247–1254.
- [21] D.D. Jayaseelan, E. Zapata-Solvas, R.J. Chater, W.E. Lee, Structural and compositional analyses of oxidised layers of ZrB_2 -based UHTCs, *J. Eur. Ceram. Soc.* 35 (2015) 4059–4071.
- [22] C.M. Chen, L.T. Zhang, W.C. Zhou, M.Q. Li, High temperature oxidation of LaB_6 - ZrB_2 eutectic in situ composite, *Acta Mater.* 47 (1999) 1945–1952.
- [23] H.B. Zhang, G.J. Zhang, J.X. Xue, J. Zhao, J.X. Liu, H.T. Liu, S.M. Peng, X.G. Long, Preparation, texturing and mechanical properties of ZrB_2 - WSi_2 ceramics via reactive hot pressing and hot forging, *Adv. Appl. Ceram.* 113 (2014) 389–393.
- [24] D.D. Jayaseelan, S. Zhang, S. Hashimoto, W.E. Lee, Template formation of magnesium aluminate ($MgAl_2O_4$) spinel microplatelets in molten salt, *J. Eur. Ceram. Soc.* 27 (2007) 4745–4749.
- [25] Z.G. Wu, W.W. Sakka, Y. Suzuki, T. Suzuki, Microstructure and anisotropic properties of textured ZrB_2 and ZrB_2 - $MoSi_2$ ceramics prepared by strong magnetic field alignment, *Int J Appl Ceram Technol.* 11 (2014) 218–227.
- [26] A. V Kovalev, E.M. Dudnik, O.N. Grigor'Ev, T.I. Shaposhnikova, I.S. Martsynyuk, Directionally solidified eutectic of the B_4C - ZrB_2 system, *Powder Metall. Met. Ceram.* 39 (2000) 63–66.

- [27] P.I. Loboda, Features of structure formation with zone melting of powder boron-containing refractory materials, *Powder Metall. Met. Ceram.* 39 (2000) 480–486.
- [28] R. Tu, H. Hirayama, T. Goto, Passive oxidation behavior of ZrB_2 -SiC eutectic composite prepared by arc melting, *Key Eng. Mater.* 403 (2008) 217–220.
- [29] M.K. Dehdashti, W.G. Fahrenholtz, G.E. Hilmas, Effects of transition metals on the oxidation behavior of ZrB_2 ceramics, *Corros. Sci.* 91 (2015) 224–231.
- [30] J. Zhou, D. Zhu, H. Zhang, I. Bogomol, S. Grasso, C. Hu, Microstructure and indentation damage resistance of ZrB_2 - 20vol.%SiC eutectic composites, *Int. J. Appl. Ceram. Technol.* 15 (2018) 619–624.
- [31] G.E.H. S. Zhu, W.G. Fahrenholtz, Influence of silicon carbide particle size on the microstructure and mechanical properties of zirconium diboride-silicon carbide ceramics, *J. Eur. Ceram. Soc.* 27 (2007) 2077–2083.
- [32] L. Zhang, N.P. Padture, Inhomogeneous oxidation of ZrB_2 -SiC ultra-high-temperature ceramic particulate composites and its mitigation, *Acta Mater.* 129 (2017) 138–148.

- ✓ Microstructural design of (UHTC) with improved the oxidation resistance
- ✓ Improved oxidation resistance is seen for melt processed $\text{ZrB}_2\text{-SiC}$
- ✓ The silica protective layer was passivating
- ✓ Melt processing allow improved design of UHTCs

ACCEPTED MANUSCRIPT